J|A|C|S
ARTICLES
Published on Web 07/14/2004

Formation of Branched Calixarene Aggregates—A Time-Resolved Static Light Scattering Study

Thomas Witte,[‡] Björn Decker,[§] Jochen Mattay,[§] and Klaus Huber*[,‡]

Contribution from the Fakultät für Naturwissenschaften, Department Chemie, Physikalische Chemie, Universität Paderborn, Warburger Strasse 100, D-33098 Paderborn, Germany, and Fakultät für Chemie, Organische Chemie I, Universität Bielefeld, Postfach 100131, D-33501 Bielefeld, Germany

Received February 6, 2004; E-mail: huber@chemie.uni-paderborn.de

Abstract: Mixtures of a calix[4]arene and a naphthyridine derivative dissolved in 1,2-dichlorobenzene form thermoreversible aggregates. The aggregation process was followed by means of time-resolved multiangle light scattering at two different mixing ratios, 1:3 and 1:4, yielding a detailed record of the relative mass, the radius of gyration, and the particle scattering function of the growing aggregates. On the basis of these data, a conclusive model of the structure is presented for the developing aggregates: monomers aggregate to wormlike filaments which form branching points. Formation of branching points proceeds in a frequency and distribution which is similar to the polycondensation of *ABC* monomers toward non-randomly branched macromolecules (Burchard, W. *Macromolecules* **1977**, *10*, 919−927). Thus, aggregation results in hyperbranched-like particles with striking analogies to the polymerization of glucose to amylopectin.

Introduction

For small molecules, the highest degree of order certainly is achieved in a three-dimensional pattern, denoted as crystal formation. From the thermodynamic point of view, this corresponds to a first-order phase transition. Although it is the most prominent example, crystallization is far from being the only process to generate ordered structures. Meanwhile, a large number of self-assembly processes have been discovered and investigated. These self-assembly processes generate supramolecular aggregates as countless and diverse as polymer science did and still does in the field of covalently linked molecules.[1,2] Although supramolecular structures are much less stable in general than macromolecules are, this instability is a strength rather than a weakness in many biological processes.[3] The inherent reversibility of these processes enables biological systems to respond in a highly flexible manner to ever-changing conditions. Therefore, such reversible processes may become an example for technical applications.

Despite characteristic differences between supramolecular structures and covalently linked polymers, analogies between the two classes of structures are striking and highly inspiring.[4] These analogies suggest application of many of the physicochemical concepts originally developed in polymer science also to the interpretation of the behavior of supramolecular structures. One of the first examples is the successful application of the concept of wormlike chains[5−7] to the aggregates of amphiphilic molecules.[8−12] Another example[13] is the interpretation of dilute solution viscosity measurements in terms of a model analoguous to the *A*−*B*-type polycondensation,[14] controllable by means of the addition of monofunctional monomers. Finally, exponents from intrinsic viscosity versus molar mass plots were successfully used by Foglman et al.[15] to extract information on the shape of aggregates.

Significant progress became possible through the use of time-resolved static light scattering (TR-SLS), which enabled an in situ recording of the growth process of aggregates. The first publications on this method reported on the investigation of ionic

[‡] Universität Paderborn.
[§] Universität Bielefeld.

(1) Among others, the following reviews give an excellent introduction into the field: (a) Fuhrhop, J.-H.; Helfrich, W. *Chem. Rev.* **1993**, *93*, 1565−1582. (b) Terech, P.; Weiss, R. G. *Chem. Rev.* **1997**, *97*, 3133−3159.
(2) (a) Lehn, J.-M. *Supramolecular Chemistry: Concepts and Perspectives*; VCH: Weinheim, Germany, 1995. (b) Lehn, J.-M. In *Supramolecular Science: Where It Is and Where It Is Going*; Ungaro, R., Dalcanale, E., Eds.; Kluwer: Dordrecht, The Netherlands, 1999.
(3) Alberst, B.; Bray, D.; Lewis, J.; Raff, M.; Roberts, K.; Watson, J. D. *The Molecular Biology of the Cell*, 3rd ed.; Garland Publishers Inc.: New York and London, 1994.
(4) (a) Brunsveld, L.; Fomer, B. J. B.; Meijer, E. W.; Sijbesma, R. P. *Chem. Rev.* **2001**, *101*, 4071−4097. (b) Ciferri, A. *Macromol. Rapid Comun.* **2002**, *23*, 511−529.
(5) Kratky, O.; Porod, G. *Recl. Trav. Chim.* **1949**, *68*, 1106−1122.
(6) Pedersen, J. S.; Schurtenberger, P. *Macromolecules* **1996**, *29*, 7602−7612.
(7) Pötschke, D.; Hickl, P.; Ballauff, M.; Astrand, P.-O.; Pedersen, J. S. *Macromol. Theory Simul.* **2000**, *9*, 345−353.
(8) (a) Imae, T.; Kamya, R.; Ikeda, S. *J. Colloid Interface Sci.* **1985**, *108*, 215−225. (b) Imae, T.; Ikeda, S. *J. Phys. Chem.* **1986**, *90*, 5216−5223.
(9) Denkinger, P.; Kunz, M.; Burchard, W. *Colloid Polym. Sci.* **1990**, *268*, 513−527.
(10) Jerke, G.; Pedersen, J. S.; Egelhaaf, S. U.; Schurtenberger, P. *Phys. Rev. E* **1997**, *56*, 5772−5788.
(11) von Berlepsch, H.; Harnau, L.; Reineker, P. *J. Phys. Chem. B* **1998**, *102*, 7518−7522.
(12) Magid, L. *J. Phys. Chem. B* **1998**, *102*, 4064−4074.
(13) Sijbesma, R. P.; Beijer, F. H.; Brunsfeld, L.; Folmer, B. J. B.; Hirschberg, J. H. K. K.; Lange, R. F. M.; Lowe, J. K. L.; Meijer, E. W. *Science* **1997**, *278*, 1601−1604.
(14) Flory, P. J. *Principles of Polymer Chemistry*; Cornell University Press: Ithaca, NY, 1953.
(15) Foglman, E. A.; Yount, W. C.; Xu, J.; Craig, S. L. *Angew. Chem.* **2002**, *114*, 4198−4200.

10.1021/ja0493291 CCC: $27.50

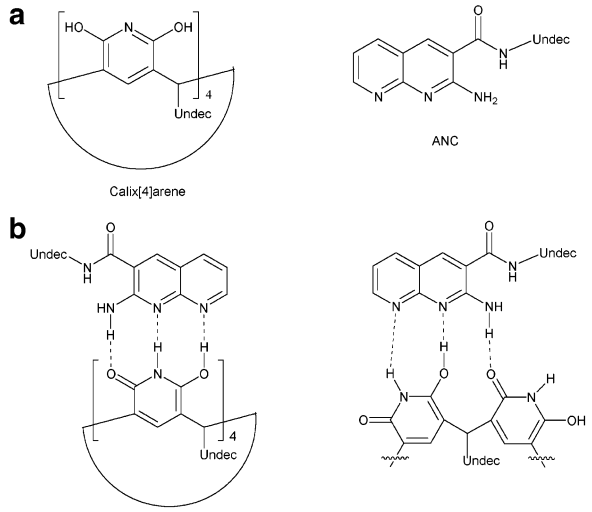

Figure 1. (a) Molecular structure of calix[4]arene and ANC. (b) Possible hydrogen bonding of aggregates between octahydroxypyridine[4]arenes and 2-amino-1,8-naphthyridines following the AAD−DDA pattern (note the octahydroxypyridine[4]arene in its tautomeric hydroxypyridone form).

dyestuffs[16−18] in dilute aqueous solution. Again, the model of wormlike chains turned out to be extremely valuable. Aside from correctly reproducing the particle shape, the wormlike chain model made it possible to discuss light scattering results without referring to mass data. This could be achieved by transforming mass values into contour lengths by means of the so-called mass per unit length.[16] However, as could also be demonstrated, this application has to be performed with great care because the onset of branching may be misinterpreted as an increased flexibility of the fibers.[17] Meanwhile, dilute solutions of a so-called dendron rod−coil molecule in 2-propanol, also investigated by TR-SLS, provided another system of reversible wormlike aggregates.[19]

Motivated by this progress, we were tempted to apply TR-SLS to the self-assembly of a completely different system. This system is composed of two components, 2,6,8,12,14,18,20,24-octahydroxy-4,10,16,24-tetra-*n*-undecylpyridine[4]arene (calix-[4]arene) and 2-amino-N^3-(*n*-undecyl)-1,8-naphthyridine-3-carboxamide (ANC). Formulas of both components are shown in Figure 1a. The present investigation succeeds earlier work which aimed at a controlled molecular aggregation[20] and which included systems involving naphthyridines.[21] Due to their AAD pattern[22] of hydrogen donor (D) and acceptor (A) groups, 2-amino-1,8-naphthyridines perfectly complement the DDA motif of octahydroxypyridine[4]arenes in their tautomeric hydroxypyridone form.[23] Following this idea, both components should form complexes especially at a 1:4 ratio of the calixarene macrocycle and naphthyridine, respectively (Figure 1b). Indeed, this was experimentally shown earlier[24] in apolar solvents such as toluene and 1,2-dichlorobenzene.

By now, a few other examples of calix[*n*]arene-based gelation have appeared in the literature. Xu et al.[25] reported on a calix-[4]arene species to which Pd(II) cations had to be added as a second component in order to induce formation of a stable "metallogel" in DMSO. However, addition of a second component is not always a necessary prerequisite for gelation. As has been shown by Shinkai et al.,[26] calix[*n*]arenes with $n = 8$ are capable of forming gels in apolar solvents by themselves. In their case, less than 1% of the calix[8]arene was required in order to induce a thermoreversible sol−gel process. Finally, we would like to draw attention to a class of water-soluble calix-[*n*]arenes.[27,28] They turned out to spontaneously form gels both in their acidic forms or as salts,[28] or after addition of lanthanides to their aqueous solutions.[27,28] As determined by dynamic light scattering, their size reached hydrodynamically effective radii as large as 225 nm, with the sodium salts persistently larger than the corresponding acids.[27] Calix[*n*]arenes also form supramolecules via inclusion of *trans*-β-carotenoid, which further aggregate to larger particles. The respective hydrodynamic radii were only 100−150 nm and thus smaller than those without the *trans*-β-carotenoid inclusion.[27]

For the system presently under investigation, shear thinning and thixotropy were observed for mixtures of calix[4]arene and ANC in molar ratios of 1:3 and 1:4. Rheological effects were much larger with the ratio 1:4. With the mixing ratio 1:4 of calix[4]arene and ANC, thermoreversible gelation could be achieved at $T = 5$ °C with concentrations of the mixture as low as 12.6 g L^{-1}.[24] In the present paper, we are aiming at the primary structures of the calix[4]arene/ANC aggregates preceding gelation by means of TR-SLS. In line with the preceding paper,[24] our experiments will be restricted to the calix[4]arene/ANC ratios 1:3 and 1:4. To make the features of single growing aggregates accessible to scattering experiments, an appropriate concentration and temperature regime had to be established first. To the best of our knowledge, we succeeded for the first time in extending the investigation of self-assembly processes by TR-SLS to the formation of nonlinear structures, and we point out similarities to a branching model well established in polymer science.

Experiments and Data Evaluation

Scattering intensities are recorded at 19 different angles θ, resulting in angular-dependent scattering curves.[29] In these curves, the scattering intensity of the aggregating particles in excess to the solvent scattering is expressed as the difference between the Rayleigh ratio of the respective calix[4]arene/ANC solutions, R_θ(CA), and the solvent background, R_θ(SB), $\Delta R_\theta = R_\theta(\mathrm{CA}) - R_\theta(\mathrm{SB}) = \Delta R(q)$. The variable of these curves is the magnitude of the scattering vector $\boldsymbol{q}$,

$$q = (4\pi n_0/\lambda)\sin(\theta/2) \qquad (1)$$

(16) Inglés, S. E.; Katzenstein, A.; Schlenker, W.; Huber, K. *Langmuir* **2000**, *16*, 3010−3018.
(17) Katzenstein, A.; Huber, K. *Langmuir* **2002**, *18*, 7049−7056.
(18) Herzog, B.; Huber, K.; Stegemeyer, H. *Langmuir* **2003**, *19*, 5223−5232.
(19) de Gans, B. J.; Wiegand, S.; Zubarev, E. R.; Stupp, S. I. *J. Phys. Chem. B* **2002**, *106*, 9730−9736.
(20) Zimmerman, S. C.; Duerr, B. F. *J. Org. Chem.* **1992**, *57*, 2215−2217.
(21) (a) Kelly, T. R.; Bridger, G. J.; Zhao, C. *J. Am. Chem. Soc.* **1990**, *112*, 8024−8034. (b) Murray, T. J.; Zimmerman, S. C. *J. Am. Chem. Soc.* **1992**, *114*, 4010−4011. (c) Brammer, S.; Lüning, U.; Kühl, C. *Eur. J. Org. Chem.* **2002**, 4054−4062.
(22) Jorgensen, W. L.; Pranata, J. *J. Am. Chem. Soc.* **1990**, *112*, 2008−2010.
(23) Gerkensmeier, T.; Näther, C.; Mattay, J. *Chem. Eur. J.* **2001**, *7*, 465−474.
(24) Gerkensmeier, T.; Decker, B.; Schwertfeger, M.; Buchheim, W.; Mattay, J. *Eur. J. Org. Chem.* **2002**, 2120−2125.
(25) (a) Xing, B.; Choi, M.-F.; Zhou, Z.; Xu, B. *Chem. Commun.* **2002**, 362−363. (b) Xing, B.; Choi, M.-F.; Zhou, Z.; Xu, B. *Langmuir* **2002**, *18*, 9654−9658.
(26) Aoki, M.; Nakashima, K.; Kawabata, H.; Tsutsui, S.; Shinkai, S. *J. Chem. Soc., Perkin Trans. 2* **1993**, 347−354.
(27) Steed, J. W.; Johnson, C. P.; Banes, C. L.; Juneja, R. K.; Atwood, J. L.; Reilly, S.; Hollis, R. L.; Smith, P. H.; Clark, D. L. *J. Am. Chem. Soc.* **1995**, *117*, 11426−11433.
(28) Makha, M.; McKinnon, I. R.; Raston, C. L. *J. Chem. Soc., Perkin Trans. 2* **2002**, 1801−1806.
(29) Becker, A.; Schmidt, M. *Macromol. Chem., Macromol. Symp.* **1991**, *50*, 249−260.

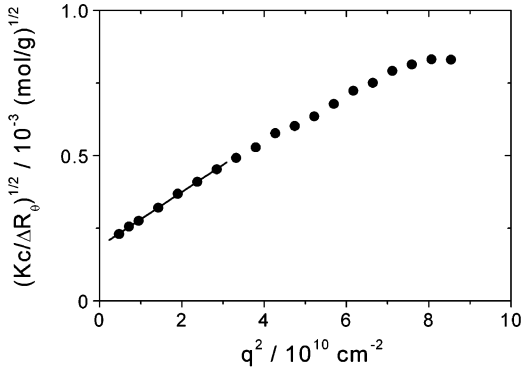

Figure 2. Data evaluation of a single curve at $t = 45$ min selected from Figure 3. The scattering curve is selected from an aggregation run of a 1:4 calix[4]arene/ANC mixture with $c = 7.61$ g L^{-1}. The mean square radius of gyration, R_g^2, is given by the slope of the curve and the relative weight-averaged molecular weight, M_w, by the limit at $q \rightarrow 0$. Curve fitting is restricted to $6.89 \times 10^{-3} \leq q \leq 1.69 \times 10^{-2}$ nm^{-1}, corresponding to the linear part of the curve.

with n_0 the refractive index of the solvent and λ the wavelength of the laser light source. Data evaluation of the scattering curves uses the inverse reduced scattering intensities $Kc/\Delta R(q)$, with K the contrast factor and c the weight in concentration of the solid (calix[4]arene with ANC) in grams per liter. In the limit of infinitely small c and q, the reduced intensity $Kc/\Delta R(q)$ yields the weight-averaged molar mass, M_w, and the z-averaged square radius of gyration, R_g^2, of the dissolved solid particles according to[30,31]

$$\frac{1}{M_w} = \lim_{\substack{c \rightarrow 0 \\ q \rightarrow 0}} \left[\frac{Kc}{\Delta R(q)} \right] \tag{2}$$

$$R_g^2 = \lim_{\substack{c \rightarrow 0 \\ q \rightarrow 0}} \left[3M_w \frac{\partial (Kc/\Delta R(q))}{\partial q^2} \right] \tag{3}$$

However, an extrapolation to $c = 0$ in eqs 2 and 3 is not possible in an aggregating system. The particle scattering factor corresponding to a normalized scattering curve was calculated by dividing the original curve by its limit at $q \rightarrow 0$, $Kc/\Delta R(q) = 1/M_w$,

$$P_z(q) = \frac{\Delta R_\theta / Kc}{\Delta R_0 / Kc} \tag{4}$$

The aggregation process is followed by measuring scattering curves at variable aggregation time t. The onset of aggregation, $t = 0$, is defined by the mixing of the two components calix[4]arene and ANC in solution.

Detailed information about the experimental procedure and the data evaluation are given in the Supporting Information.

Results and Discussion

Evolution of Particle Size. Solutions of calix[4]arene/ANC in the present investigation led to aggregation processes which could be followed by means of TR-SLS for at least 60 min. The power of this method is illustrated in Figure 3, representing a selection of scattering curves from a single run. Each curve results in a value for the relative mass, M_w, and the size, R_g. Figures 4 and 5 show the development of the radius of gyration, R_g, and the relative weight-averaged molar mass, M_w, as functions of time for the 1:4 and 1:3 mixtures, respectively. For both mixing ratios, the growth process is accelerated if the concentration of the calix[4]arene/ANC mixture is increased. Aggregation of all 1:4 mixtures is faster, leading to larger particles than aggregation in solutions of the corresponding 1:3 mixtures does. Although this is represented in a double logarithmic plot, no clear-cut power laws became discernible in Figures 4 and 5.

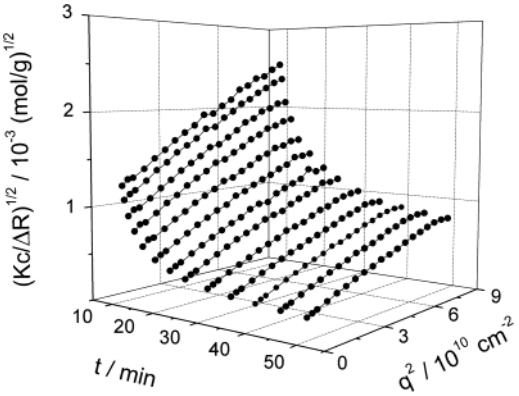

Figure 3. Berry plot of a selection of scattering curves for a 1:4 calix[4]arene/ANC mixture with $c = 7.61$ g L^{-1}.

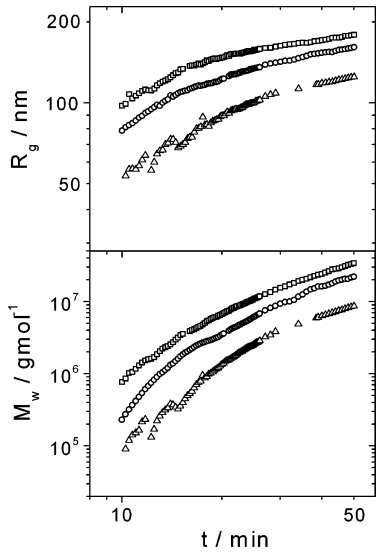

Figure 4. Development of the radius of gyration, R_g, and the relative weight-averaged molar mass, M_w, as a function of time for the 1:4 mixtures at $c = 7.61$ (□), 6.97 (○), and 6.34 g L^{-1} (△).

However, focusing on the initial and final stages of the respective aggregation processes, limiting exponents can be discussed for $R_g \propto t^{\alpha_t}$. At the onset of aggregation, exponents were close to $\alpha_t = 0.75$ for 1:4 mixtures and $\alpha_t = 1.4$ for 1:3 mixtures. In the case of the final stage, located at aggregation times of $t \geq 30$ min, exponents were found to be $0.19 \leq \alpha_t \leq 0.26$ for the 1:4 mixtures and $0.33 \leq \alpha_t \leq 0.52$ for the 1:3 mixtures.

Those limiting exponents can be compared with the growth laws of two prominent model processes for fractal aggregates, diffusion-limited cluster aggregation (DLCA) and reaction-limited cluster aggregation (RLCA). In these model processes, not only do monomers add to aggregates but particles at any degree of aggregation, denoted as clusters, stick to any other cluster. Both processes may serve as possible models for the aggregation of calix[4]arene and ANC. Noticeably, the exponents at the final stages of the aggregation do not even get close to the theoretical value, $\alpha_t \propto 1/d_f = 1/1.8$, which corresponds

(30) (a) Zimm, B. *J. Chem. Phys.* **1948**, *16*, 1093−1099. (b) Zimm, B. *J. Chem. Phys.* **1948**, *16*, 1099−1116.
(31) Berry, G. C. *J. Chem. Phys.* **1966**, *44*, 4550−4564.

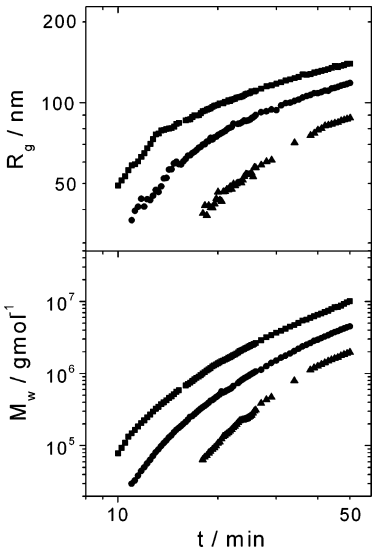

Figure 5. Development of the radius of gyration, R_g, and the apparent weight-averaged molar mass, M_w, as a function of time for the 1:3 mixtures at $c = 6.53$ (■), 6.00 (●), and 5.45 g L^{-1} (▲).

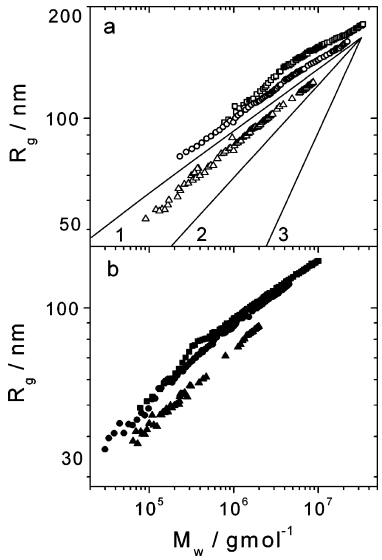

Figure 6. (a) Radii of gyration, R_g, versus the apparent mass, M_w, for the 1:4 mixture at $c = 7.61$ (□), 6.97 (○), and 6.34 g L^{-1} (△). The curves describe trends of R_g versus M_w for particle formation of spheres (1), coils (2), and rods (3), where the average values include the monomer fraction, respectively. (b) Radii of gyration, R_g, versus the apparent mass, M_w, for the 1:3 mixtures at $c = 6.53$ (■), 6.00 (●), and 5.45 g L^{-1} (▲). For the higher concentrations, at least two linear regimes became distinguishable.

to the respective inverse fractal or Hausdorf dimension expected for DLCA.[32,33] Exponents at the initial stages were significantly larger than 1/1.8. If at all, the only structural hint is provided by the initial exponents from the 1:4 mixtures being close to 1, which may indicate an initial formation of linear objects with an almost constant growth rate. Finally, the curves in Figure 4 do not support the exponential growth (not shown explicitly) of $R_g \propto e^{ct}$ predicted for the RLCA.[33,34]

Further insight into the mechanism of particle formation is expected to be obtained if the radius of the growing particles is related to the respective increase of the relative particle mass. Such a relation is shown in Figure 6, where the *z*-averaged root-mean-squared radius of gyration, R_g, is plotted versus the apparent weight-averaged mass, M_w, for all three concentrations of both mixtures. In the case of self-similar systems, such a plot leads to a power law of

$$R_g \propto M_w^{\alpha_g} \tag{5}$$

The most prominent examples are rods ($\alpha_g = 1.0$), polymeric coils[14] ($\alpha_g = 0.5-0.6$), and spheres ($\alpha_g = 0.33$). For clusters from DLCA[32,33] and from RLCA,[33,34] exponents of $\alpha_g \approx 0.57$ and 0.48, respectively, are predicted. For the calix[4]arene/ANC system, a single power law could be identified only at the lowest concentrations respectively, resulting in $\alpha_g = 0.19$ for the 1:4 mixture and $\alpha_g = 0.24$ for the 1:3 mixture. At higher concentrations, at least two regimes became distinguishable, indicating two stages of the growth process with the corresponding exponents extending over a range of $0.12 < \alpha_g < 0.21$ for the 1:4 mixtures and $0.18 < \alpha_g < 0.31$ for the 1:3 mixtures. Thus, all experimental slopes are much smaller than α_g of any of the above-mentioned self-similar systems.

Yet, only distributions of clusters resulting from DLCA or RLCA can unambiguously be ruled out as possible model systems. The three other examples for self-similar systems have to be considered more carefully. If the calix[4]arene/ANC aggregates consist of growing rods, coils, or spheres, growth may occur at the expense of monomers, which gradually attach to the aggregates. In such cases, the M_w values available from eq S5 (Supporting Information) and used in eq 5 correspond to overall mass values, which include the monomers. This is due to the fact that evaluation of M_w by means of eq S5 is based on a constant overall concentration, *c*, corresponding to the original weight in quantity. On the other hand, power laws require averaged mass data which exclusively refer to the aggregates. Such aggregate mass values could be calculated from eq S5 only if separate concentrations were measurable for the mass fractions of monomers and of aggregates, respectively, at all intermediate stages[18] of the aggregation process. Unfortunately, such data are not available.

To account explicitly for a decreasing amount of monomers, we calculated R_g versus M_w curves which include the respective monomer fractions for all three self-similar systems. For simplicity, we assumed that monodisperse rods, coils, or spheres are formed. Consideration of a polydispersity for the developing aggregates would only result in a parallel shift of the trends and would be of no relevance for our qualitative discussion. Monomer length and monomer weight were adopted to generate systems comparable in size to the present aggregates. Details are given in the Supporting Information. The calculated systems still form self-similar particles but are not self-similar as a whole due to the coexistence of the monomers. As a consequence, those systems no longer lead to unique exponents α_g. However, we are still able to compare trends in the size and mass regime under consideration. Corresponding trends are expressed in terms of intermediate exponents, which are $\alpha_g \approx 0.50$ (rods), 0.25 (coils), and 0.17 (spheres). These intermediate exponents are half of the exponents of the corresponding power laws in the "particle-only" limit. As is demonstrated in Figure 6, neither the theoretical trend for rods nor coils is small enough to

(32) Weitz, D. A.; Huang, J. S.; Lin, M. Y.; Sung, J. *Phys. Rev. Lett.* **1984**, *53*, 1657−1660.
(33) Weitz, D. A.; Huang, J. S.; Lin, M. Y.; Sung, J. *Phys. Rev. Lett.* **1985**, *54*, 1416−1419.
(34) Lin, M. Y.; Lindsay, H. M.; Weitz, D. A.; Ball, R. C.; Klein, R.; Meakin, P. *Phys. Rev. A* **1990**, *41*, 2005−2020.

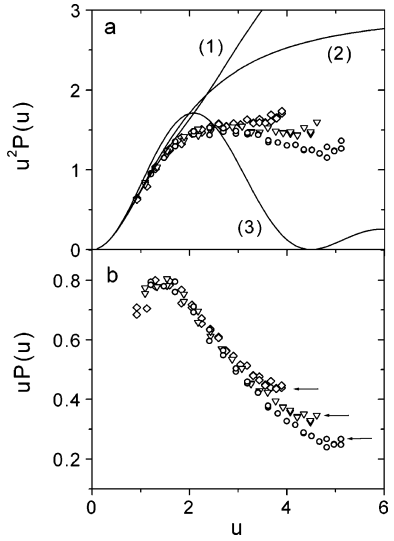

Figure 7. (a) Kratky plot of three scattering curves for a 1:4 mixture with $c = 7.61$ g L^{-1} at $t = 15$ (◇), 25 (▽), and 45 min (○). All curves show an upturn in the scattering curve for $q > 2.5 \times 10^{-2}$ nm^{-1}. (b) Holtzer plot of the same data as in (a). The scattering factor approaches a power law of $P(q) \propto q^{-1}$ for $q > 2.5 \times 10^{-2}$ nm^{-1}, typical for rodlike structures (indicated by arrows).

reproduce the observed experimental curves. Thus, comparison with experiments may provide a first hint for the formation of compact particles. In the section to follow, we take advantage of the fact that we can discuss results without referring to mass values. As will be outlined, this is achieved by a procedure which transforms M_w data into L_w and in which the above-mentioned problem caused by the use of overall concentrations is canceled.

Particle Shape. To get additional information on the shape of the growing particles, particle scattering factors are analyzed in a final step. If a dimensionless and normalized variable u,

$$u = qR_g \tag{6}$$

is used instead of q, all scattering curves of a self-similar system fall on top of each other. Examples of such systems are polymer coils, rods, and spheres. In Figure 7, theoretical curves of these systems are compared with three experimental curves. The experimental curves were recorded at three different times during the growth of the 1:4 mixture with $c = 7.61$ g L^{-1}. Three major aspects become apparent: (i) None of the three models generates a scattering curve comparable to those of the calix[4]arene/ANC aggregates. (ii) All experimental curves form a single trend, indicating similar shapes for all intermediates. Noticeably, the experimental curves represented as Kratky plots, $u^2P(u)$ versus u, exhibit a shallow maximum at $u \approx 2.5$. Such maxima are typical for rather compact structures such as branched macromolecules. (iii) All curves in Figure 7a show an upturn in the scattering curve for $q > 2.5 \times 10^{-2}$ nm^{-1}.

We first pay attention to the maximum value observed in Figure 7a with the Kratky plot. This maximum is compatible with various types of branched structures. An overview of the scattering behavior of the most prominent branching models was given by Burchard[35] in 1983, comprising (i) stars with f numbers of rays equal in length;[36] (ii) stars with f rays having a distribution of their length;[37] (iii) randomly branched polycondensates of the A_f type with a functionality f of the monomer;[38] (iv) non-randomly branched polycondensates of the *ABC* type[39] where *A* can only react with *B* or *C*, including the special case of $B = C$;[40] and (v) a loosley branched microgel denoted as soft sphere.[41] For non-randomly branched structures (iv), the term "hyperbranched" is used alternatively.

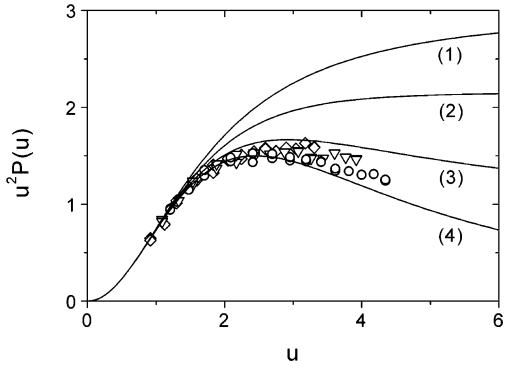

Figure 8. Kratky plot for an *f*-functional randomly branched polycondensate of the A_f type with $C = 1$ (1), and three curves of the non-randomly branched *ABC* polycondensation model[40] for $C = 0.3$ (2), $C = 0.1$ (3), and $C = 0$ (4). Theoretical curves are compared with the same selection of scattering curves used in Figure 7 (1:4 mixture of calix[4]arene/ANC with $c = 7.61$ g L^{-1}). The q regime is restricted to $q < 2.5 \times 10^{-2}$ nm^{-1}, corresponding to $u < 3.33$, $u < 3.94$, and $u < 4.37$, respectively.

As pointed out by Burchard,[40] distinction among some of the models becomes possible by means of the Kratky representation of the particle scattering behavior. Whereas star branched molecules and nonrandom polycondensates exhibit a maximum value in this plot, random polycondensates and linear chains do not. To interpret our scattering data in terms of branching models, we compared experiments with theoretical predictions based on two models as a "first guess". The comparison is outlined in Figure 8, which includes a selection of experimental scattering curves as $u^2P(u)$ together with the model curve of the randomly branched A_f type and three non-randomly branched *ABC* polycondensates. The three *ABC* types differ in the branching parameter C defined by eq S14 (Supporting Information). Variation of the parameter C is achieved by varying the reactivity β of the *B* groups and the reactivity γ of the *C* groups with the *A* groups, respectively. It has to be emphasized that $\beta = \gamma$ corresponds to the nonradom *ABB* type. In Figure 8, two different values for the C parameter and the limit of large extent of reaction of the *A* groups for $C = 0$ were calculated. In Figure 9, a sketch of an *ABC* polycondensate is shown. Details of the calculations are given in the Supporting Information. In fact, description of the experimental curves by the *ABC* type with $0 < C < 0.1$ is fairly good as long as we exclude the q regime of $q > 2.5 \times 10^{-2}$ nm^{-1}, which is characterized by an upturn in the Kratky plot. The height of the maximum in the Kratky representation led to a further differentiation. Regular stars with monodisperse rays have lower maximum values than nonrandom polycondensates and stars with a length distribution of the arms. They can thus be excluded as potential candidates for the aggregates under the present investigation.

(35) Burchard, W. *Light scattering from polymers*; Advances in Polymer Science 48; Springer: Berlin/Heidelberg, 1983.
(36) Benoit, H. *J. Polym. Sci.* **1953**, *11*, 507−510.
(37) Burchard, W. *Macromolecules* **1974**, *7*, 835−841.
(38) Kajiwara, K.; Burchard, W.; Gordon, M. *Br. Polym. J.* **1970**, *2*, 110−115.
(39) Burchard, W. *Macromolecules* **1972**, *5*, 604−610.
(40) Burchard, W. *Macromolecules* **1977**, *10*, 919−927.
(41) Burchard, W.; Kajiwara, K.; Nerger, D. *J. Polym. Sci. Part B: Polym. Phys.* **1982**, *20*, 157−171.

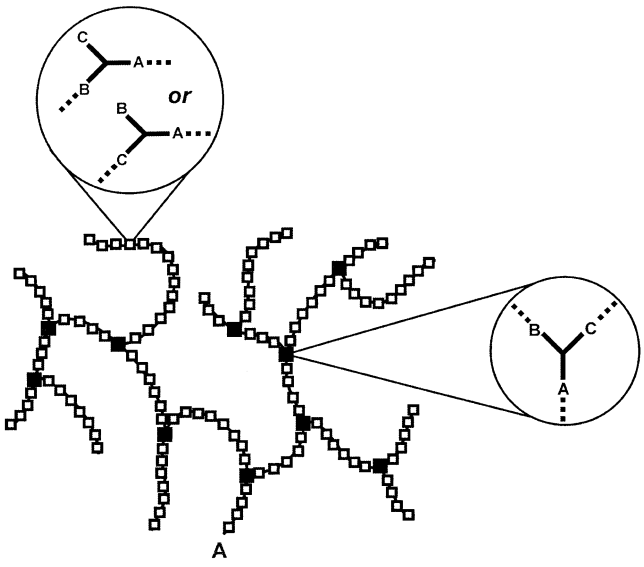

Figure 9. Sketch of an *ABC* polycondensate. The branching points consist of three reacted groups, whereas the linear segments exhibit two reacted groups only.

Finally, we direct our attention to the high q regime of the experimental scattering curves in Figure 7. As is demonstrated in Figure 7b, the upturn of the Kratky plots turns into the onset of a plateau if the so-called bended-rod plot ($uP(u)$ versus u) is used. A plateau of $qP(q)$ corresponds to a power law of $P(q) \propto q^{-1}$, which is typical for rodlike structures[42,43] and semiflexible chains.[44] Under the assumption that this plateau is significant, we estimated the corresponding heights by multiplying the original scattering data at $2.75 \times 10^{-2} < q < 2.92 \times 10^{-2}$ nm^{-1} by the magnitude of the scattering vector, q. According to eq 7, this gives access to a mass per unit length, M_L, via[45]

$$q\frac{\Delta R_\theta}{Kc} = \pi M_L = \pi\frac{M_w}{L_w} \qquad (7)$$

where L_w is the weight-averaged contour length of the particles.

Prior to any application of eq 7, two aspects have to be emphasized: (i) Branching does not affect the unambiguous determination of the contour length.[17] If branching occurs, all linear segments contribute to the overall contour length, L_w. (ii) Theoretically, the q^{-1} power law of particle scattering factors is reached at $u > 1$ for monodisperse rods and at $u > 2$ for polydisperse rods. Assuming the contour lengths, L_w, of the rodlike constituents to be twice as large as the aggregate radius, R_g ($L_w = 2R_g$), at the most, a lower particle size limit $R_{g(low)}$ for the applicability of eq 7 can be estimated. This estimation has to be related to the high q regime accessible to the present instrument ($2.75 \times 10^{-2} < q < 2.92 \times 10^{-2}$ nm^{-1}) and is based on $u = 2 = qR_{g(low)} = qL_w/\sqrt{12}$, yielding $R_{g(low)} = 2/q \approx 80$ nm and $L_w = 300$ nm. On the basis of these arguments, we restricted application of eq 7 to scattering curves with $R_g > 100$ nm. In fact, all scattering curves selected according to this criterion exhibited an onset of a q^{-1} power law. Only in the case of $c = 5.45$ g L^{-1} of the 1:3 mixture, all radii remained below this size limit and could not be used for calculating M_L values.

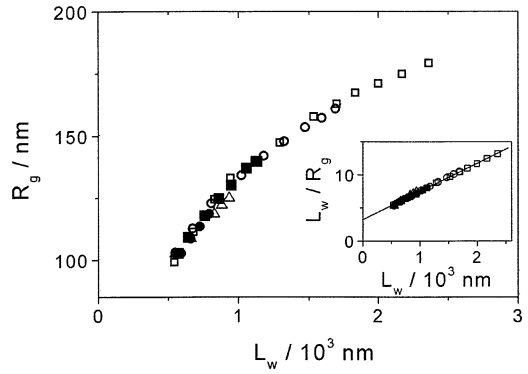

Figure 10. Radii of gyration, R_g, versus the overall contour length, L_w, for 1:4 mixtures with $c = 7.61$ (□), 6.97 (○), and 6.34 g L^{-1} (△) and for 1:3 mixtures with $c = 6.53$ (■) and 6.00 g L^{-1} (●). Inset: Same data plotted as L_w/R_g vs L_w. Data can be extrapolated to $L_w/R_g = 3.21$, indicating rodlike aggregates.

Although not shown explicitly, the apparent values for M_L extracted according to eq 7 exhibit a gradual increase with L_w. As was demonstrated earlier,[18] this reflects either an increase of the cross section of the fiber-like constituents or an increase of an apparent mass per unit length due to an increasing number of linear aggregates (with a large scattering power) at the expense of a gradual loss of monomers (with a very low scattering power) at a constant overall value of c in eqs 2 and S5. The resulting mass per unit length lies within a range of $1500 < M_L < 15\,000$ g mol^{-1} nm^{-1}. Assuming a density of 1 g mL^{-1}, this results in fiber cross sections D of $1.8 < D < 5.6$ nm. Because the monomers contribute to c, the estimated M_L range establishes a lower limit. Yet, these values are realistic and point to fiber cross sections which comprise several monomeric strands.

Once values for the mass per unit length are established, they can be transformed into weight-averaged contour lengths, L_w, by inserting mass values into eq 7. These contour lengths can be related to the particle size (Figure 10) in much the same way as was done for the relative molar mass, M_w, in Figure 6a,b. Yet, contrary to M_w, the contour length L_w is not affected by the use of overall concentrations in eqs 2 and S5, and remaining deviations from the true values for L_w can arise only from the influence of interparticular excluded volume effects, which are considered to be negligible in the present case.

Most strikingly, R_g data of all concentrations and mixtures now fall on a single line. This success confirms the onset of a q^{-1} decrease of $P(q)$ at $q > 2.75 \times 10^{-2}$ nm^{-1} and at the same time can be considered to be a justification for the applicability of eq 7. As a consequence, the same topological features can be assumed for all mixing ratios and solute concentrations. An additional hint about the structure of the constituents can be extracted from an alternative representation of the data in Figure 10. This representation is initiated by the fact that, for rodlike paritcles, $L/R_g = \sqrt{12}$. In fact, a plot of L_w/R_g versus L_w yields a straight line, which can be extrapolated to 3.21, indicating rodlike aggregates to be the initial aggregates or constituents.

By combining the two structural features just established, the following model is proposed for the aggregates. On large length scales, the aggregates behave like hyperbranched polymers. On

(42) Neugebauer, T. *Ann. Phys.* **1943**, *42*, 509−533.
(43) Holtzer, A. *J. Polym. Sci.* **1955**, *17*, 432−434.
(44) Koyama, R. *J. Phys. Soc. Jpn.* **1973**, *34*, 1029−1038.
(45) Schmidt, M.; Paradossi, G.; Burchard, W. *Makromol. Chem. Rapid Commun.* **1985**, *6*, 767−772.

decreasing the length scale, the focus turns toward linear segments between branching points, which correspond to rather stiff fibers.

The character of hyperbranching became transparent by the scattering curves at $q < 2.5 \times 10^{-2}$ nm^{-1}. In this q regime, the respective experiments could be well described by the Gaussian limit of the *ABC* polycondensate, with R_g and C in eq S13 being the only fit parameters. We have to emphasize that, in this limit, all intraparticular distances of the model obey a Gaussian distance distribution. This feature certainly gets increasingly unrealistic with decreasing intraparticle distances and increasing chain stiffness. The character of stiff fiber-like constituents is supported by the onset of $P(q) \propto q^{-1}$ for $q > 2.75 \times 10^{-2}$ nm^{-1} and by a ratio of $R_g/L_w \approx 1/\sqrt{12}$ in the limit of small aggregates.

Conclusions

At this stage we can only speculate about the details of intermolecular interactions which cause the aggregation process under consideration. However, due to the typical dependence of the aggregates on the solvent polarity, we assume an interaction according to the AAD−DDA pattern[22] (Figure 1b). Since the 2-amino-1,8-naphthyridine has an amide function in its 3-position, an additional cross-linking between small assemblies should be possible, leading to aggregates of high molecular weight. Furthermore, the arrangement of four naphthyridine units at the upper rim of the calixarene might cause severe steric hindrance, resulting in a rearrangement under formation of cross-linked aggregates. Further studies to elucidate the oriented bond formation between neighboring constituents of these calixarene aggregates by experimental and theoretical methods are in progress.

However, we succeeded in following the time-resolved aggregation process of calix[4]arene/ANC in 1,2-dichlorobenzene by TR-SLS. Aside from demonstrating the power of TR-SLS in the field of aggregation, we were able to offer a structural model for the calix[4]arene-based aggregation in solution. Without referring to a specific particle shape, we could use the onset of a $qP(q)$ plateau to attribute contour lengths, L_w, to the particles. All radii of aggregating intermediates fall on a single curve if plotted versus this total contour length, L_w, independent of the concentrations and compositions of calix[4]arene/ANC mixtures. Angle-dependent scattering curves compared best with a model curve for a non-randomly branched *ABC* polycondensate with a branching parameter of $0 < C < 0.1$. This corresponds to non-randomly branched polymers with a large extent of reaction α. On the basis of these findings, we postulate the following scheme of particle formation for the calix[4]arene/ANC aggregates in 1,2-dichlorobenzene: Monomers aggregate to fiber-like filaments, which form branching points. Each branching point initiates the growth of at least two other filaments. It is noteworthy that a strikingly similar structure was proposed recently for two different low-molecular-weight gelators.[46,47] In the present system, the branching points occur in a frequency and distribution which is similar to those for nonrandom *ABC* polycondensates in macromolecular chemistry. Unlike the original model, which is based on a Gaussian distance distribution between any two segments, the bridges between two branching points are very stiff. Although resolution of the actual aggregation mechanism requires a detailed analysis of all scattering curves in terms of the respective model parameters of the *ABC*-type polycondensate, it is noteworthy that aggregates of calix[4]arene/ANC mixtures reveal striking analogies to the polymerization of glucose to amylopectin[48,49] or to the formation of a hyperbranched polyester.[50]

Acknowledgment. This work is dedicated to the memory of Professor Walther H. Stockmayer. Many helpful discussions with Professor Walther Burchard are gratefully acknowledged. The authors are indebted to Matthias Fornefeld for assistance in the laboratory.

Supporting Information Available: Experimental procedures and data evaluation, formulas for the calculation of the R_g versus M_w curves of monomer/aggregate mixtures, and equations of the scattering factor for the *ABC*-type polycondensates. This material is available free of charge via the Internet at http://pubs.acs.org.

JA0493291

(46) Liu, X. Y.; Sawant, P. D. *Appl. Phys. Lett.* **2001**, *79*, 3518−3520.
(47) Liu, X. Y.; Sawant, P. D.; Tan, W. B.; Noor, I. B. M.; Pramesti, C.; Chen, B. H. *J. Am. Chem. Soc.* **2002**, *124*, 15055−15063.
(48) Hanselmann, R.; Burchard, W.; Ehrat, M.; Widmer, H. M. *Macromolecules* **1996**, *29*, 3277−3282.
(49) Galinsky, G.; Burchard, W. *Macromolecules* **1997**, *30*, 4445−4453.
(50) De Luca, E.; Richards, R. W.; Grillo, I.; King, S. M. *J. Polym. Sci. Part B: Polym. Phys.* **2003**, *41*, 1352−1361.